Journal of ELECTRONIC MATERIALS, Vol. 35, No. 3, 2006 *Regular Issue Paper*

Influence of Ni Concentration and Ni_3Sn_4 Nanoparticles on Morphology of Sn-Ag-Ni Solders by Mechanical Alloying

HSIANG-YI LEE[1] and JENQ-GONG DUH[1,2]

1.—Department of Materials Science and Engineering, National Tsing Hua University Hsinchu, Taiwan 300, Taiwan. 2.—E-mail: jgd@mx.nthu.edu.tw

The mechanical alloying (MA) process was employed as an alternative method to produce the lead-free solder pastes of Sn-3.5Ag-xNi (x = 0.1, 0.5, 1.0, 1.5, and 2.0) in this study. When the Ni concentration was low (x = 0.1, 0.5), MA particles agglomerated to a flat ingot with particle sizes >100 μm. For higher Ni concentration (x = 1.0, 1.5, and 2.0), MA particles turned into fragments with particle sizes <100 μm. The particle size of the solders appeared to be dependent on the Ni concentration. To reduce the particle size of SnAgNi alloys with low Ni concentration, Ni_3Sn_4 nanoparticles were doped into Sn and Ag powders to derive a Ni_3Sn_4-doped solder. For the Ni_3Sn_4-doped solder, the particle size was smaller than that doped by the pure Ni. The distinction of milling mechanism between Ni_3Sn_4-doped solder and the pure Ni-doped solder by MA process was probed and discussed. In addition, differential scanning calorimetry (DSC) results ensured its feasibility in applying the solder material in the reflow process. Wettability tests between solders and Cu substrate also revealed that the wetting angles for Ni_3Sn_4-doped solder with low Ni concentration (0.1 and 0.5 wt.%) were smaller than those for pure Ni-doped solder. The wetting angles on both Cu substrate and electroplated Ni metallization for SnAgNi solders were also comparable with commercial Sn-3.5Ag and Sn-3.0Ag-0.5Cu solders. Favorable wettability of the as-derived solder in this study was clearly demonstrated.

Key words: Mechanical alloying (MA), Ni_3Sn_4 nanopowders, Sn-Ag-Ni solder, wettability

INTRODUCTION

In the manufacture of electronic package systems, solders play a crucial role in the interconnection of silicon die. Because the solder provides the electrical and mechanical connection between silicon die and bonding pad, the material selection for solder alloys continues to be a key factor. Due to environmental and public health concerns, lead-free soldering is now a global trend in electronic packaging.[1–8] Lead-free solders are mostly based on eutectic Sn-3.5Ag alloys, including SnAg, SnAgCu, SnAgBi, and SnAgIn, in which these alloys are doped with small additions of other elements, such as Fe, Co, and Ni.[9–17] An additional element or a second phase has been added into Sn-3.5Ag solders to improve such properties as melting temperature, mechanical strength, mechanical fatigue resistance, creep resistance, and solder joint reliability.[16–19]

Nickel was recently chosen to modify the interfacial properties of the solder joint in both Sn-3.5Ag and Sn-37Pb systems.[20–23] The microstructure of interfacial reactions varied with Ni composition. The addition of Ni led to distinct Cu_6Sn_5 regions at the interface, and the morphology of Cu_6Sn_5 changed with the Ni content.[23] Therefore, the controllability and the ingenuity of Ni in fabricating solder materials for accurate composition is essential.

Many methods have been used to produce solder alloys, and the mechanical alloying (MA) technique is one of them. By the process of repeated welding, fracturing, and rewelding powder particles, MA produces defects and boundaries that reach homogeneity at room temperature, and it works well especially in the mixture of low- and high-melting temperature elements. The characteristics of the MA process have been studied.[24–27] In milling powder mixtures

(Received March 1, 2005; accepted October 26, 2005)

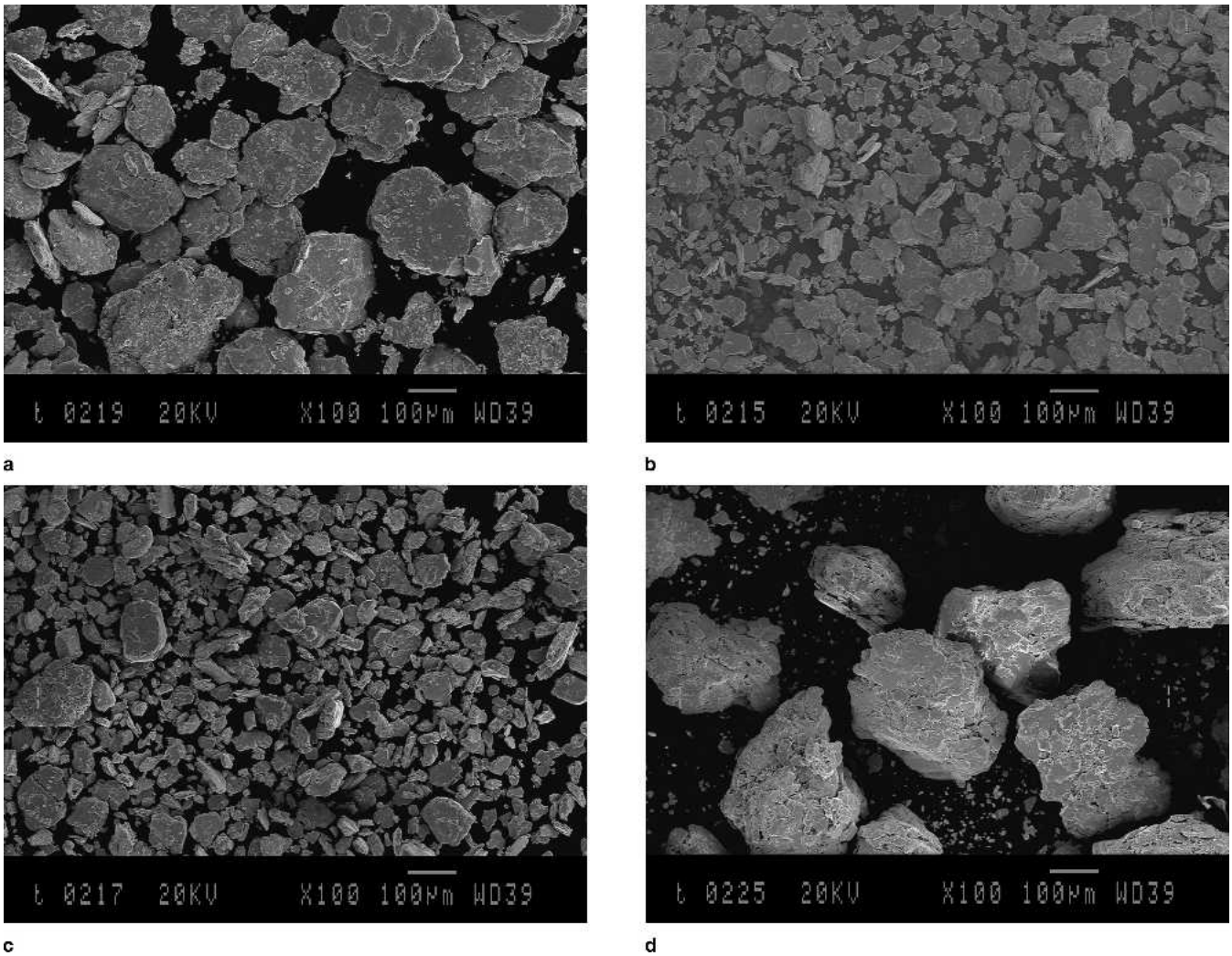

Fig. 1. SEI micrographs of 94.5Sn-3.5Ag-2.0Ni MA powders after various milling times: (a) 10, (b) 20, (c) 30, and (d) 50 hr.

of ductile and brittle components, the ductile metal powder particles are flattened while the brittle particles are fractured to smaller fragments. These fragmented brittle particles become trapped in the ductile particles.[24] During the milling process, the lamellar structure is further refined, and the brittle particles tend to be uniformly dispersed in the ductile matrix. If the solubility of brittle components in

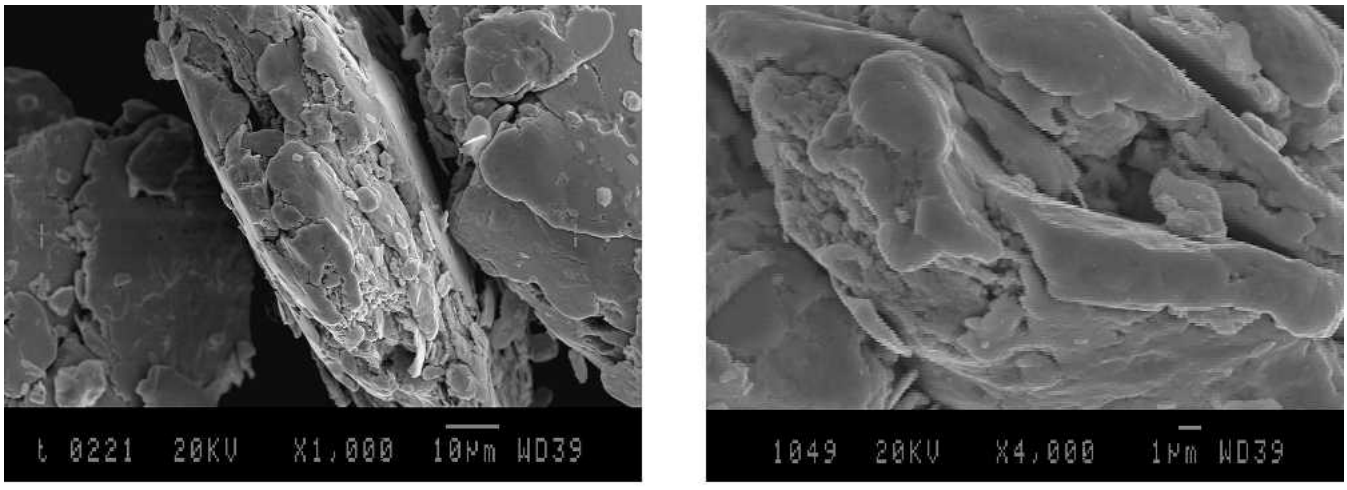

Fig. 2. SEI micrographs of detailed microstructure of the 94.5Sn-3.5Ag-2.0Ni MA powders milled after various times: (a) 10 and (b) 20 hr.

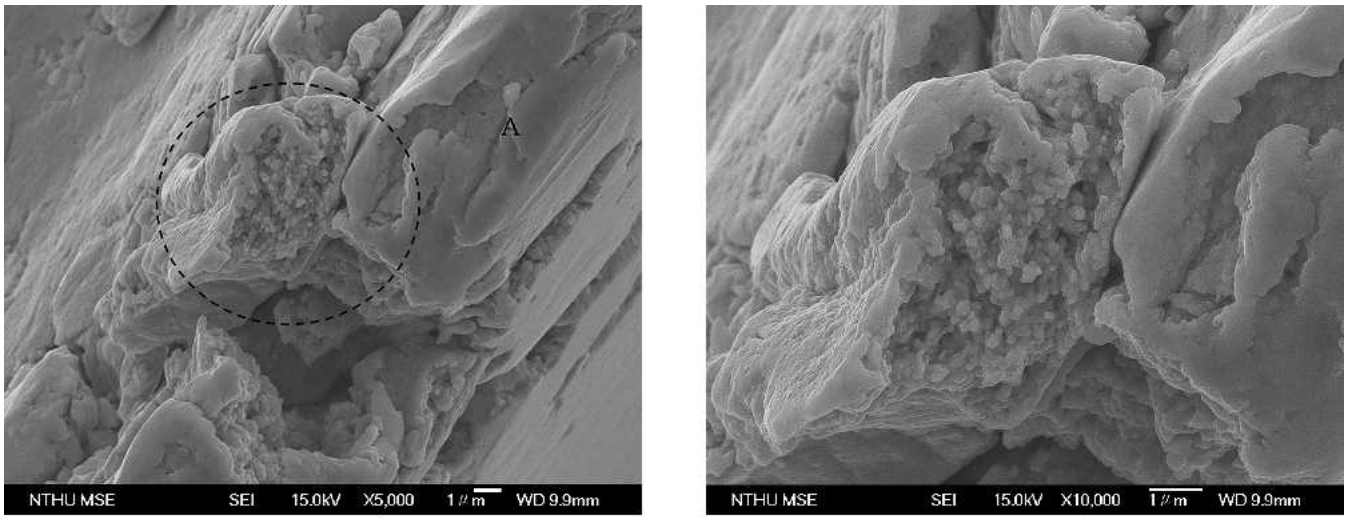

a b

Fig. 3. SEI micrographs of 94.5Sn-3.5Ag-2.0Ni MA powders after 30 hr of milling: (a) cold-welded region (A), and (b) enlarged view inside the circle in (a) exhibiting the composite lamellar structure.

the ductile matrix is sufficient, alloying occurs.[27] The concentration of elements in the mixture can be controlled, and solder pastes can be easily produced by direct addition of flux.

SnAgNi powders were fabricated by the MA technique for this study. The influence of milling time and Ni concentration on powder morphologies and particle size was investigated. Various milling times were selected to search for the optimum conditions in MA process. The aim was to decrease the particle size to <100 μm effectively, and Ni_3Sn_4 nanoparticles were thus added to fracture the larger-alloy powders. Furthermore, the melting temperatures of Ni-doped and Ni_3Sn_4-doped alloy powders were evaluated to test the feasibility for soldering process.

EXPERIMENTAL PROCEDURES

Starting materials were Sn (-100 mesh, purity 99.85 wt.%), Ag (5–8 μm, 99.9 wt.%), and Ni (5–10 μm, >99 wt.%) powders in this study. Three kinds of powders were deposited in a zirconia container, and milling balls of either 1 cm or 3 mm in diameter were used. The ball-to-powder weight ratio was maintained at 26:1. Alcohol was added into the powders as a surfactant to reduce excessive cold welding. To investigate the influence of Ni contents on the morphology of SnAgNi solder powder, the total weight of input powder was fixed to 5 g, and the amount of Ni was varied from 0.1 to 2.0 wt.%. Mechanical alloying was performed at room temperature in a high-energy milling planetary ball mill (Pulverisette 5, Fritsch GmbH, Idar-Oberstein, Germany) with a rotation speed of ~190 rpm.

Morphologies of MA powders after various milling times were observed. The milling times were chosen as 10, 20, 30, and 50 hr. Alloy phases and crystal structures of MA powders were identified with a x-ray diffractometer (D/MAX-B, Rigaku, Tokyo, Japan)

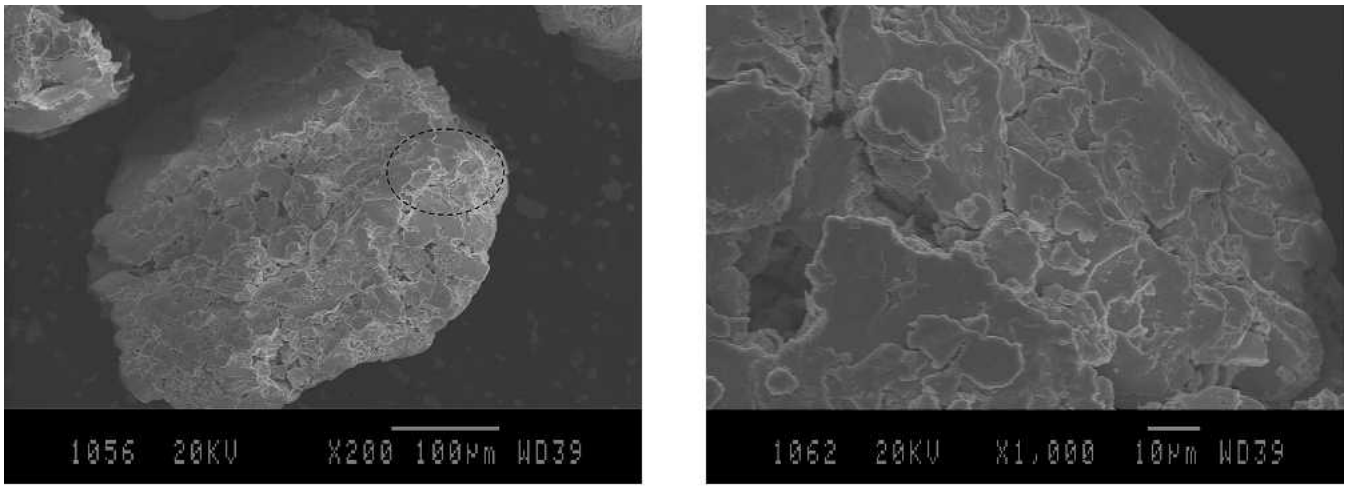

a b

Fig. 4. SEI micrographs of 94.5Sn-3.5Ag-2.0Ni MA powders milled for 50 hr: (a) low-magnification view; (b) enlarged view of (a) showing that flakes that had started to aggregate and that stacked to form lumps.

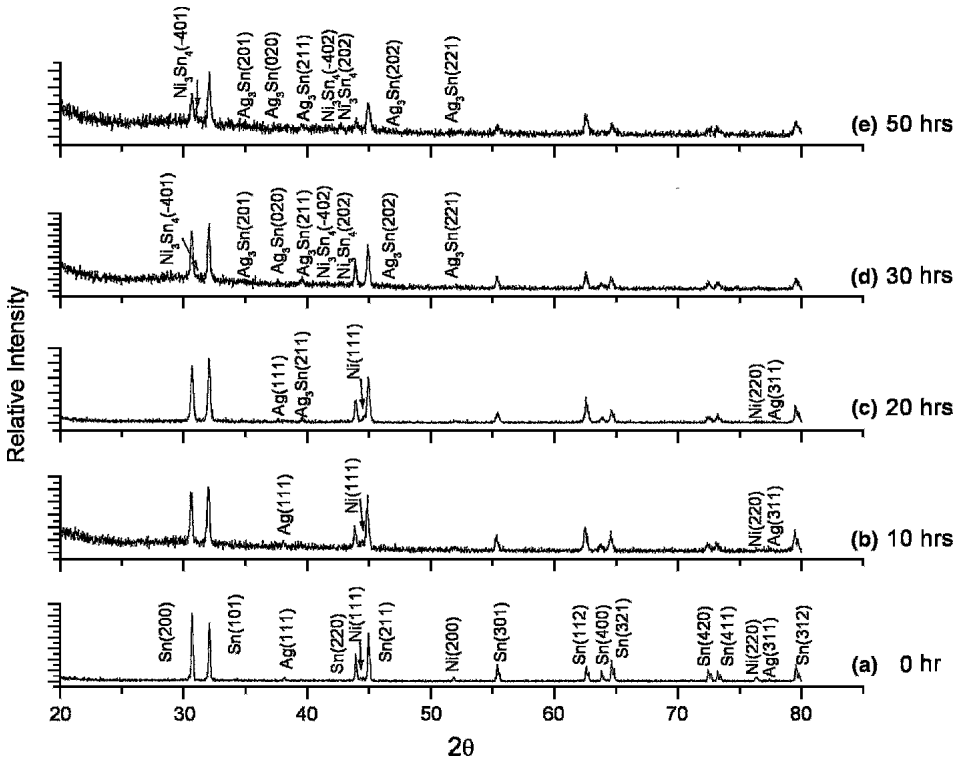

Fig. 5. X-ray diffraction peaks of 94.5Sn-3.5Ag-2.0Ni powders, (a) as-prepared, and milled for various periods of time: (b) 10, (c) 20, (d) 30, and (e) 50 hr.

using Cu Kα with a wavelength of λ = 1.5406 Å. To demonstrate the compatibility of soldering process, a DSC tester (Model 6200, Seiko, Tokyo, Japan) was used to measure the melting point of as-fabricated solder powders. MA powders were heated at a rate of 10°C/min. under an Ar atmosphere. To ensure the homogeneity, compositions of the MA powder were analyzed with an inductively coupled plasma-atomic emission spectrometer (ICP-AES, Optima 3,000 DV, PerkinElmer, Boston, MA). A dynamic contact-angle analyzer system was used to measure the contact angle of the solder pastes on Cu/Si and electroplated Ni/Cu/Si. The Cu/Si and electroplated Ni/Cu/Si with solder pastes were put into the heated environment chamber. During the melting process, live images were continuously captured. From the live images, the contact angle could be measured.[28]

Nanoscale Ni_3Sn_4 powders were synthesized by chemical methods, which involved reducing a solution of $Ni(NO_3)_2$ and $SnSO_4$. $NaBH_4$ solution was added to the solution containing Ni and Sn ions. Upon addition of the $NaBH_4$ solution, a black precipitate was immediately observed. The black

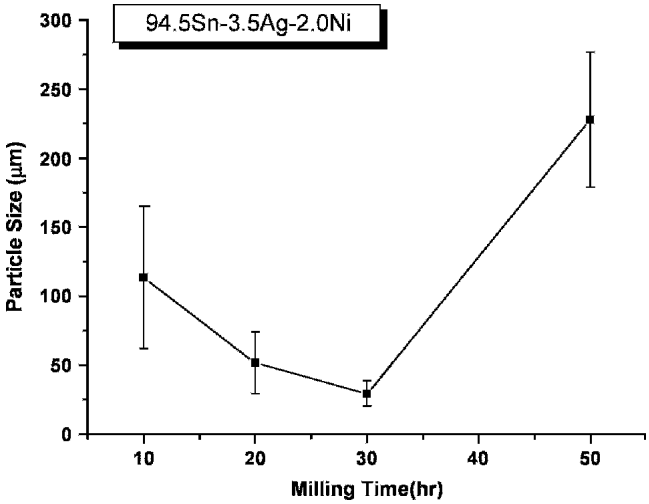

Fig. 6. Particle size of 94.5Sn-3.5Ag-2.0Ni MA powders as a function of milling time.

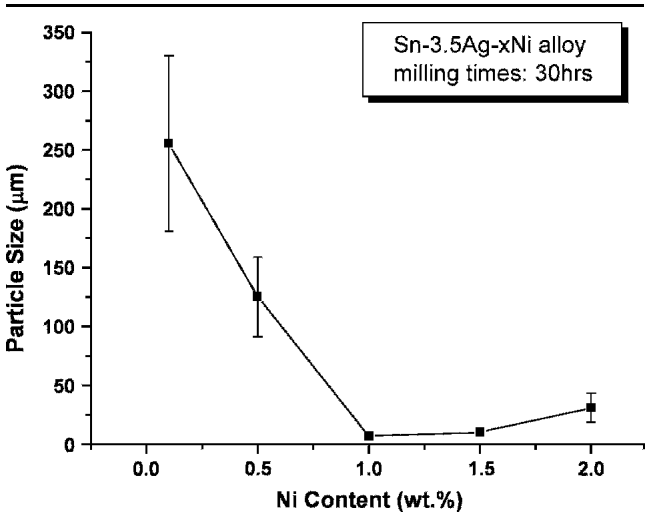

Fig. 7. Particle size of Sn-3.5Ag-xNi with various Ni content milled for 30 hr; x = 0.1, 0.5, 1.0, 1.5, and 2.0 wt.%.

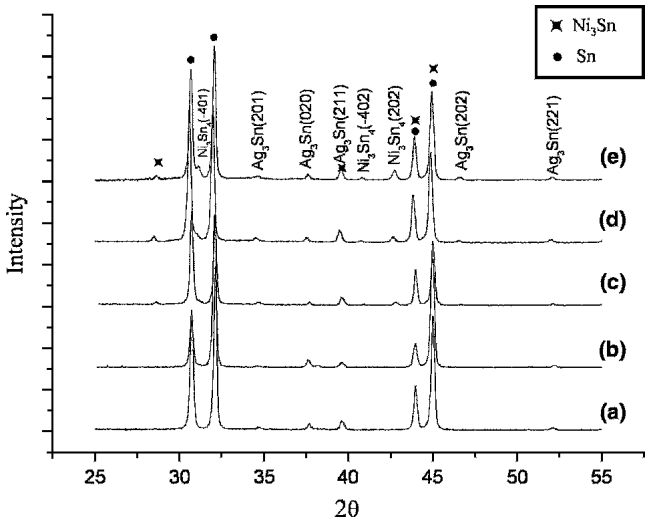

Fig. 8. X-ray diffraction peaks of Sn-3.5Ag-xNi powders milled for 30 hr, for various Ni contents: (a) x = 0.1, (b) x = 0.5, (c) x = 1.0, (d) x = 1.5, (e) x = 2.0 wt.%.

Table I. Onset Temperature of Sn-3.5Ag-xNi Powders Measured by Differential Scanning Calorimetry Tester

Ni Content (wt.%) in Sn-3.5Ag-xNi	Onset Temperature (°C)
0.1	218.06 ± 0.8
0.5	218.73 ± 0.7
1.0	217.98 ± 0.9
1.5	216.88 ± 0.6
2.0	217.44 ± 0.7
96.5Sn-3Ag-0.5Cu solder manufactured by arc melting[16]	~217

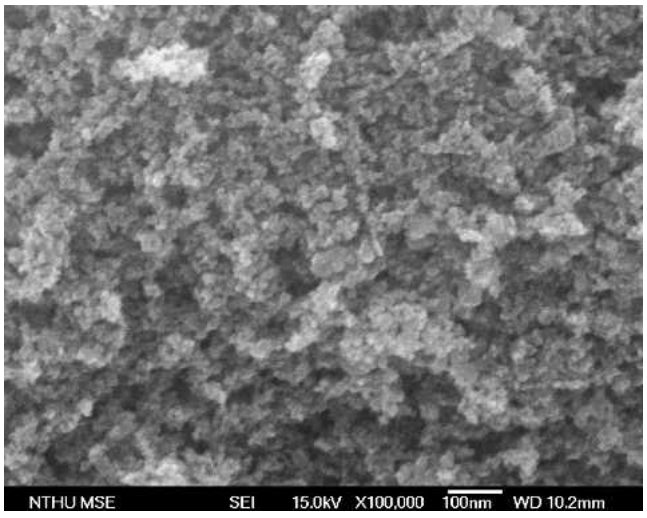

Fig. 9. SEI micrograph of the Ni_3Sn_4 nanopowders.

precipitate was washed with distilled water and then dipped in alcohol at room temperature. The particle size, shape, and morphology of milled MA powders were observed with a field-emission scanning electron microscope (FESEM, JSM-6500F, JEOL, Tokyo, Japan). Various ratios of Ni to Ni_3Sn_4 powders were deposited with Sn and Ag in the zirconia container. After the powders had been milled for 10 hr, the morphologies of the MA powders were further examined.

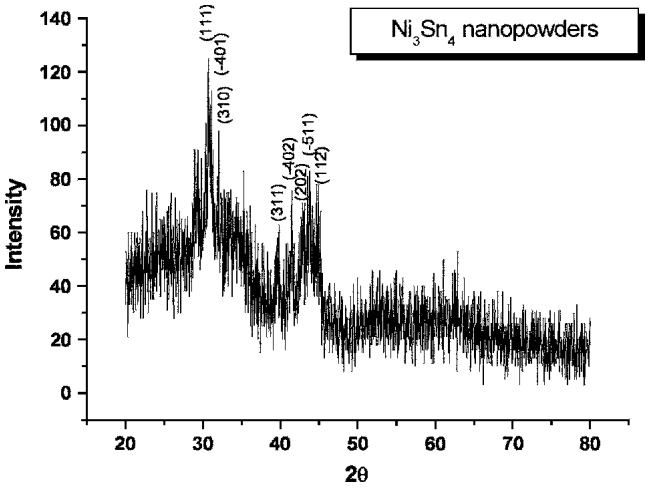

Fig. 10. X-ray diffraction peaks of the chemically produced Ni_3Sn_4 nanopowders.

Table II. Average Particle Size of 94.5Sn-3.5Ag-2.0Ni MA Powders Milled after 10 hr with Different Ni-to-Ni_3Sn_4 Powder Ratios*

No.	Ni (%)	Ni_3Sn_4 (%)	Average Particle Size (μm)
1	100	0	79.01 ± 33.8
2	75	25	7.72 ± 3.92
3	50	50	5.45 ± 2.68
4	25	75	5.37 ± 2.25
5	0	100	3.56 ± 1.93

*The total weight percent of Ni and Ni_3Sn_4 is 2.0 wt.%.

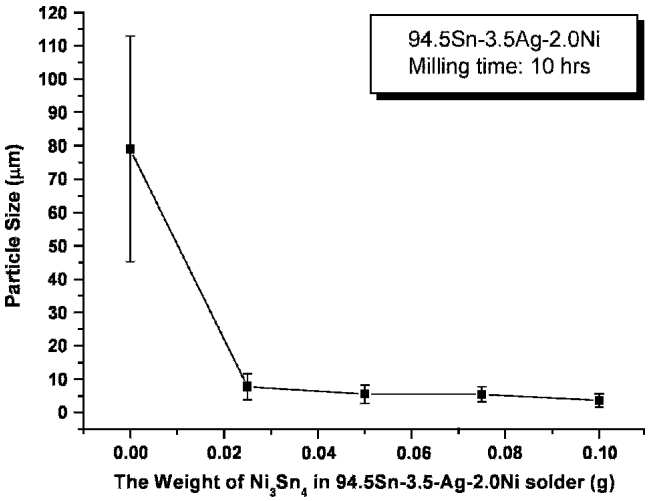

Fig. 11. Particle size of 94.5Sn-3.5Ag-2.0Ni with various Ni_3Sn_4 contents milled for 10 hr; total amount of Ni and Ni_3Sn_4 is 2.0 wt.%.

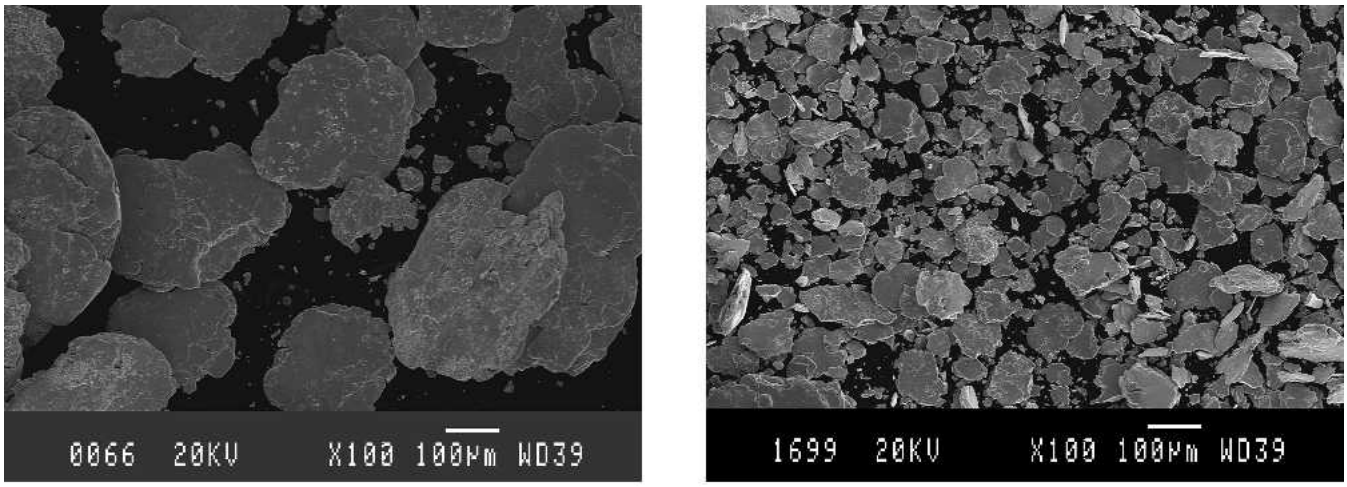

a b

Fig. 12. SEI micrographs of 96.4Sn-3.5Ag-0.1Ni MA powders produced by milling with (a) SnAgNi and (b) SnAg(Ni_3Sn_4) nanopowders for 30 hr.

RESULTS AND DISCUSSION

Characteristics of MA Powders and Milling Mechanisms

To produce the lead-free solder powders of SnAgNi by MA, various milling times were selected. After 10 hr of milling, the powders were pressed to thin and flat plates with size of ~100 μm. For another 10 hr, the plates were flattened to much thinner dimensions and fractured to even smaller pieces. When milled for 30 hr, powders were shattered to flakes, and then aggregated to chunks for up to 50 hr, as shown in Fig. 1.

Different mechanisms for the MA process have been proposed.[27–30] Because Sn and Ag are ductile materials and accounted for >95% of compositions in this study, the ductile particles were flattened and cold welded to sheets when milled below 20 hr, as indicated in Fig. 2. It was revealed that Ni particles tended to be wrapped inside, possibly because the hardness of nickel is higher than that of Ag and Sn.[31,32] With continuous milling, the crystal defects and refined structure would enhance the diffusion rate at low temperature, leading to phase transformation and dissolution.[24,33] A recent study of the Sn-3.5Ag system by the MA process showed that Ag dissolved into the grain boundaries and the intermetallic phase of Ag_3Sn was formed.[28,30] This phenomenon was also found in the Sn-3.5Ag-xNi system in this study, in which not only Ag_3Sn was formed but also Ni_3Sn_4 was found. Because the hardness of the Ni_3Sn_4 alloy phase is higher than the matrix composed with Sn and Ag,[31–32] the Ni_3Sn_4 phase would be wrapped in the matrix and then dispersed homogeneously.

Figure 3 shows a composite lamellar structure of the constituent metals, which were formed after further milling and thus cold welded. During high-energy ball striking, dislocations and defects were formed and work hardening consequently occurred. By the process of work hardening and Ni_3Sn_4 dispersion, SnAgNi powders began to fracture and

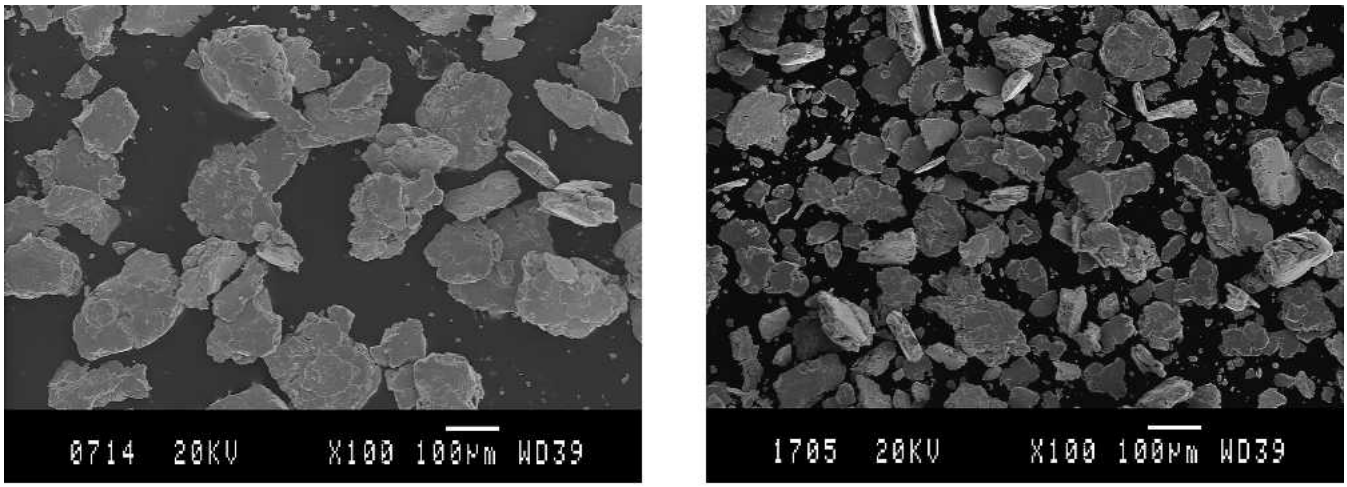

a b

Fig. 13. SEI micrographs of 96Sn-3.5Ag-0.5Ni MA powders produced by milling with (a) SnAgNi and (b) SnAg(Ni_3Sn_4) nanopowders for 30 hr.

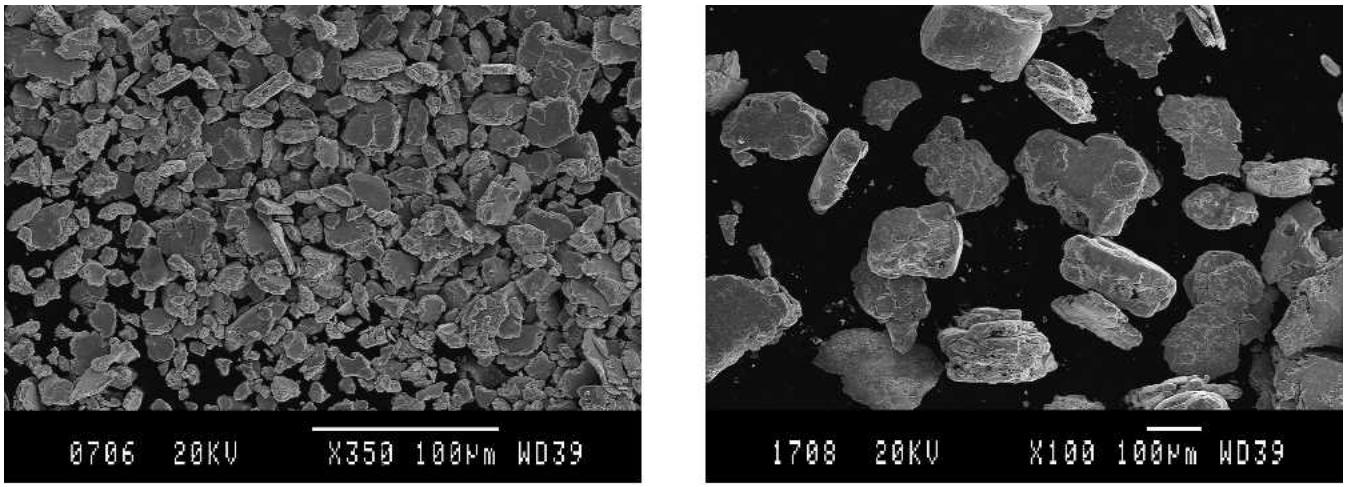

a b

Fig. 14. SEI micrographs of 95.5Sn-3.5Ag-1.0 Ni MA powders produced by milling with (a) SnAgNi and (b) SnAg(Ni_3Sn_4) nanopowders for 30 hr.

thus particle size was decreased. When milled above 30 hr, fractured flakes started to aggregate and stacked to lumps, as indicated in Fig. 4.

To ensure the existence of alloy phases during the MA process, x-ray diffraction peaks of various milling times were evaluated, as shown in Fig. 5. After milling more than 30 hr, the x-ray peaks of Ag and Ni all disappeared and Ag_3Sn and Ni_3Sn_4 were formed. If the milling time is rather short, Ag and Ni will not effectively dissolve into Sn, and the effect of work hardening and Ni_3Sn_4 dispersion will not be appreciable.

Figure 6 presents the particle size for various milling times. The particle size decreased with the milling time in the range of 10–30 hr. It should be pointed out that the deviation of measured particle size is large for 10 hr milling due to the inefficient work hardening and Ni_3Sn_4 dispersion, as mentioned above. However, the particle size would increase again when milled more than 30 hr. In fact, powders started to aggregate and they formed stacks if milled too long, and the particle size became too large. Therefore, the milling time was chosen to be 30 hr in consideration of smaller particle size and detection of evidence of alloy phases.

Influence of Ni Concentration on Morphology of SnAgNi Solders

Figure 7 shows the particle size distribution of Sn-3.5Ag-xNi MA powders. When the concentration of doped Ni was >1.0 wt.%, the average particle size was <100 μm. The amounts of Ni_3Sn_4 alloy wrapped and dispersed in the matrix would increase with Ni contents after 30 hr of milling. Therefore, the effect of grinding and fracture would be enhanced by MA process. The presence of Ni_3Sn_4 was identified with the aid of XRD results.

The result of XRD demonstrated the evidence of Ni_3Sn_4 formation during the MA process. In Fig. 8, Ag_3Sn phase was detected in the Sn-3.5Ag-xNi system after 30 hr of milling. Besides, when Ni concentration was as high as 1.0 wt.%, Ni_3Sn_4 formed and Ni_3Sn was also detected. The particle size decreased as the Ni concentration increased to 1.0 wt.%.

The fracture of ductile alloy powders and the reduction of particle size could be attributed to the formation of Ni_3Sn. It was argued that approximate amounts of Ni and Sn particles were mixed and cold welded together to form Ni_3Sn_4 alloy phase. Besides, more Ni particles milled with Sn particles should lead to the formation of Ni_3Sn alloy phase. It

Table III. ICP-AES Results of Sn-3.5Ag-xNi Solder Powders Milled after 30 hr with the MA Process

Solder Type	Alloy Designation	Nominal Ag and Ni Concentration	ICP-AES Measured Concentration (wt.%)	
			Ag	Ni
Ni-doped solder	M01	3.5Ag-0.1Ni	3.35 ± 0.28	0.10 ± 0.04
	M05	3.5Ag-0.5Ni	3.50 ± 0.39	0.48 ± 0.17
	M10	3.5Ag-1.0Ni	3.50 ± 0.27	0.95 ± 0.21
	M15	3.5Ag-1.5Ni	3.48 ± 0.35	1.51 ± 0.12
	M20	3.5Ag-2.0Ni	3.51 ± 0.53	1.98 ± 0.13
Ni_3Sn_4-doped solder	C01	3.5Ag-0.1Ni	3.47 ± 0.42	0.10 ± 0.06
	C05	3.5Ag-0.5Ni	3.43 ± 0.33	0.53 ± 0.09
	C10	3.5Ag-1.0Ni	3.45 ± 0.28	0.88 ± 0.12

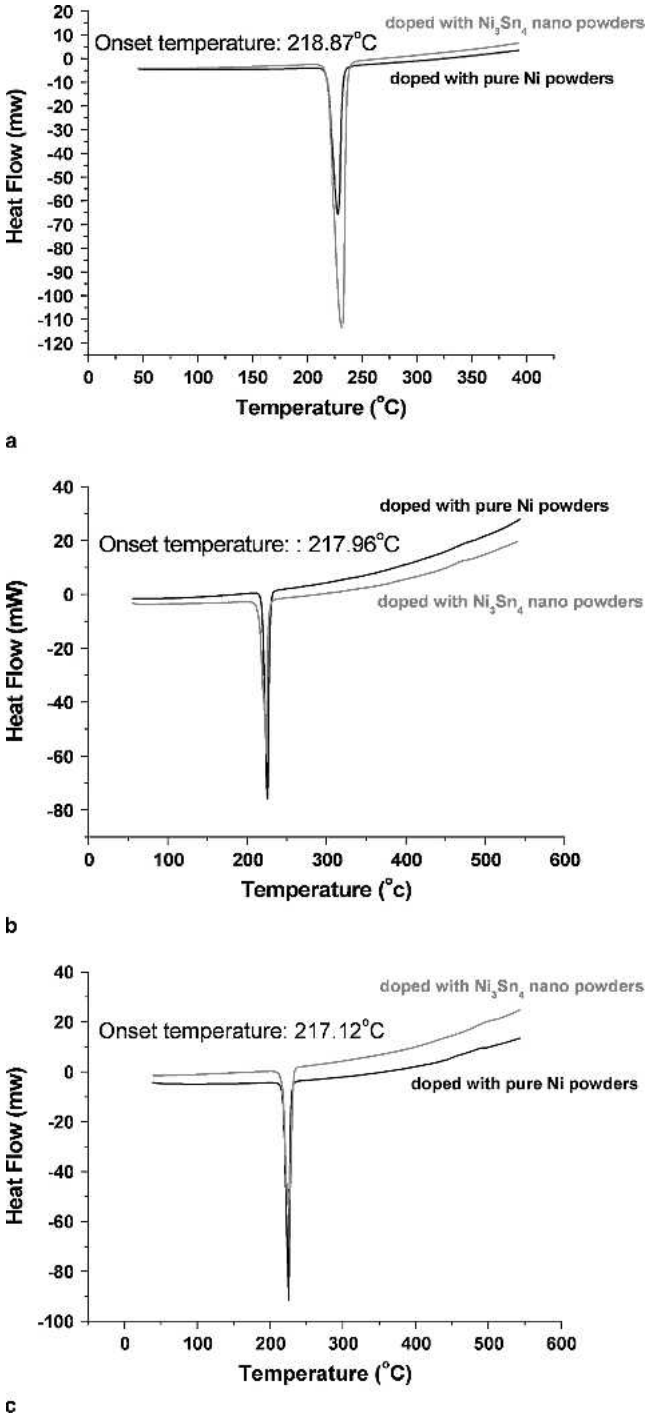

Fig. 15. DSC profiles of Sn-3.5Ag-xNi MA powders milled for 30 hr with various Ni contents: (a) x = 0.1, (b) x = 0.5, and (c) x = 1.0 wt.%.

is believed that as more NiSn alloys formed, greater amounts of hard alloys were dispersed in the matrix during milling. Therefore, the effect of fracture was enhanced.

For the soldering process, the melting temperature of solders is a crucial parameter, because it is the main factor in deciding the process temperature. Measured melting points of Sn-3.5Ag-xNi MA powders after 30 hr milling are shown in Table I. With Ni content ranging from 0.1 to 2.0 wt.%, variation in the melting point is not appreciable during the MA process. This implies that the solder temperature would not be altered, even if different SnAgNi solders with various Ni contents were modified by the MA technique.

Effect of Ni_3Sn_4 Doping on Morphology of SnAgNi Solders

In practice, the large size of the SnAgNi solder alloy fabricated by the MA process was not appropriate for current solder-bump technology. Therefore, modifications in the MA process to decrease the particle size were needed. As indicated above, the particle size of Sn-3.5Ag-xNi solder alloy was reduced due to the formation and dispersion of Ni_3Sn_4 during the MA process. A mechanism of ductile–brittle materials by the MA process has been proposed.[30] When brittle particles were doped into ductile particles, they would be trapped in the ductile particles after milling. With further milling, brittle particles will disperse in the ductile matrix homogeneously. For this reason, MA powders are more brittle, and the fracture effect will be so predominant that size can be further decreased.

Because the hardness of Ni_3Sn_4 is higher than the matrix, introducing Ni_3Sn_4 into the solder powders should be an additive effect on MA process.[32] Ni_3Sn_4 nanopowders $<$100 nm were produced by a chemical participation method. Figure 9 shows the SEI micrograph of Ni_3Sn_4 nanopowders, and the corresponding XRD is presented in Fig. 10.

To study the influence of Ni_3Sn_4 nanopowders upon SnAgNi solder alloy, various Ni_3Sn_4-to-Ni ratios were designed and doped into Sn and Ag powders, followed by milling for 10 hr. The total amount of Ni_3Sn_4 and Ni was 2.0 wt.%. The short milling time was chosen to ensure striking of Ni_3Sn_4 on the SnAgNi alloy and also to prevent the small pieces from untimely formation and aggregation. The results of evaluated average particle size are presented in Table II and Fig. 11. It appears that the particle size decreased abruptly when a small amount of Ni_3Sn_4 was doped into SnAgNi solder powders after 10 hr of milling. This is the evidence of Ni_3Sn_4 striking on SnAgNi alloy, forming Ni_3Sn_4-doped solder during high-energy ball milling.

Figures 12–14 exhibit the morphologies of Ni-doped and Ni_3Sn_4-doped powders. The alloy designations are listed in Table III. In comparing the particle size between Ni_3Sn_4 and Ni-doped solders with the identical Ni content, it is revealed that the particle size of Ni_3Sn_4-doped solder C01 (Sn-3.5Ag-0.1Ni) and C05 (Sn-3.5Ag-0.5Ni) decreased to 10–50 μm after 30 hr of milling. On the other hand, the size of C10 (Sn-3.5Ag-1.0Ni) became larger than that of Ni-doped solders M01, M05, and M10. When 1.0 wt.% Ni_3Sn_4 was doped into Sn3.5Ag solder, the striking effect was so strong that shatters formed prematurely and aggregated together in continuous milling, as revealed in Fig. 14. Therefore, the particle size would increase due to aggregation. SEM micrographs demonstrate the fracturing effect of Ni_3Sn_4

Table IV. Contact Angles of Various MA Solders and Commercial Solders on Cu/Si and Electroplated Ni at 240°C

Designation	Solders	Wetting Angle (deg)	
		Cu Substrate	Electroplated Ni
Ni-doped solder paste	Sn3.5Ag	24 ± 0.5	22 ± 0.3
	Sn3.5Ag0.1Ni	23 ± 0.3	18 ± 0.2
	Sn3.5Ag0.5Ni	2 ± 0.3	19 ± 0.1
	Sn3.5Ag1.0Ni	22 ± 0.4	21 ± 0.2
	Sn3.5Ag1.5Ni	21 ± 0.5	20 ± 0.6
	Sn3.5Ag2.0Ni	20 ± 0.6	16 ± 0.4
Ni_3Sn_4-doped solder paste	Sn3.5Ag0.1Ni	18 ± 0.2	18 ± 0.3
	Sn3.5Ag0.5Ni	15 ± 0.4	19 ± 0.2
	Sn3.5Ag1.0Ni	25 ± 0.6	20 ± 0.4
Commercial solder paste	Sn3.5Ag	26 ± 0.5	22 ± 0.6
	Sn3.0Ag0.5Cu	25 ± 0.3	25 ± 0.4

on SnAgNi solder alloy fabricated by the MA process. The milling mechanism of the ductile–brittle materials is evident once more.

In addition, the DSC curves in Fig. 15 reveal that no other endothermic peak was found, indicating the complete melting of MA powders below 240°C. The reduced melting point made the powders workable as solder pastes during reflows. The melting point of the Sn-3.5Ag-0.1Ni MA powders doped with Ni_3Sn_4 was 218.87°C, which is close to that of Ni-doped MA powders previously listed in Table I. For Ni_3Sn_4 doping up to 1.0 wt.%, the melting points of these MA powders maintained in the range from 217 to 219°C, as indicated in Fig. 15. Therefore, MA particle size can be reduced to <100 μm by doping Ni_3Sn_4 nanopowders, and a suitable melting point of the Ni_3Sn_4 doped MA particles ($\leq$1.0 wt.% Ni_3Sn_4) ensured feasibility for applications in solder-bump technology. It is interesting to point out that the onset temperatures of MA solder in this study was comparable to those of Sn-3Ag-0.5Cu and Sn-3Ag-0.5Cu-0.1X (X=Fe, Ti, Mn, Ni, and Co) solders manufactured by traditional methods, as listed in Table I.[16] All of these solders show similar onset temperatures around 217–218°C.

Successive milling would make the alloy more homogeneous. To confirm homogeneity after 30 hr of milling, Ni and Ag concentrations analyzed by ICP-AES for the SnAgNi solder alloy produced by the MA process are listed in Table III. The measured concentration of the as-fabricated solder powders was close to the nominal one. To ensure the accuracy in measurement, each composition was measured by ICP six times, and the average results are presented in Table III.

Wetting Properties of SnAgNi Solders on Different Types of UBM

To ensure good bonding between solders and substrates, wetting is an essential prerequisite for soldering. Therefore, the contact angles of solder powders prepared by MA on Cu(5 μm)/Si and electroplated Ni/Cu/Si were measured.

The solder powders prepared by the MA process were added by flux and then applied on Cu/Si and electroplated Ni/Cu/Si before wettability test. Contact angles of SnAgNi solders on the metallization layer are listed in Table IV. These solder pastes were derived from three different routes, including (1) doping pure Ni by MA process, (2) doping Ni_3Sn_4 by MA process, and (3) Sn-3.5Ag and Sn-3.0Ag-0.5Cu commercial solder pastes. The contact angles of MA solder pastes were revealed to be close to those of commercial solder pastes on both Cu/Si and electroplated Ni/Cu/Si. The contact angles of MA powders were all $<25°$, and their wettabilities were all comparable to the commercial one.

Table IV shows that the contact angles of solder pastes on electroplated Ni metallization are smaller than those on Cu substrate. The wetting properties of solder pastes on the electroplated Ni metallization were better than that of Cu substrate. In addition, the wettability between Ni_3Sn_4-doped solders and Cu substrate for the SnAgNi solder pastes decreased with Ni_3Sn_4 doping ($\leq$0.5 wt.%). In fact, the contact-angle data of both the MA solder and the composite solder fabricated in this study exhibits favorable wettability.

CONCLUSIONS

The Sn, Ag, and Ni powders were mixed, and the SnAgNi solder alloy tended to be flattened and cold welded in the early stages of the MA process. With increasing milling time, powders were shattered to flakes and then aggregated to chunks when milling times were longer than 50 hr. The particle size would decrease due to the formation of Ni_3Sn_4 alloys, which were wrapped and dispersed in the matrix, and thus the MA powders became more brittle.

The XRD results of Sn-3.5Ag-xNi solder powders demonstrated that not only Ni_3Sn_4 formed but also Ni_3Sn was detected. The brittle property of Ni_3Sn_4 caused the fracture of the ductile alloy powders, and smaller particle sizes resulted. By doping nanosized Ni_3Sn_4 particles into original MA powders and then milling for 30 hr, the particle size of solder powders decreased significantly from 150~200 to 10~50 μm.

In addition, the melting points of Ni-doped solders were 217–219°C, which was comparable to that of Ni_3Sn_4-doped solders. Slight Ni_3Sn_4 doping made contact angles between solders and Cu substrate become smaller. The contact angles of MA powders on both Cu/Si and electroplated Ni/Cu/Si were $<25°$. Therefore, MA-derived powders could be employed as solder materials for the subsequent reflow process.

ACKNOWLEDGMENT

Financial support from National Science Council, Taiwan, under contract NSC-93-2216-E-007-014 is acknowledged.

REFERENCES

1. T.Y. Lee, W.J. Choi, K.N. Tu, J.W. Jang, S.M. Kuo, J.K. Lin, D.R. Frear, K. Zeng, and J.K. Kivilahti, *J. Mater. Res.* 17, 291 (2002).
2. D.R. Frear, J.W. Jang, J.K. Lin, and C. Zhang, *JOM* 53, 28 (2001).
3. W.H. Tao, C. Chen, C.E. Ho, W.T. Chen, and C.R. Kao, *Chem. Mater.* 13, 1051 (2001).
4. S.K. Kang et al., *J. Electron. Mater.* 30, 1049 (2001).
5. J.W. Jang, D.R. Frear, T.Y. Lee, and K.N. Tu, *J. Appl. Phys.* 88, 6359 (2000).
6. P.T. Vianco et al., *J. Electron. Mater.* 28, 1127 (1999).
7. M.E. Loomans and M.E. Fine, *Metall. Mater. Trans. A* 31, 1155 (2000).
8. T.M. Korhonen, P. Su, S.J. Hong, M.A. Korhonen, and C.Y. Li, *J. Electron. Mater.* 29, 1194 (2000).
9. F. Guo, S. Choi, J.P. Lucas, and K.N. Subramanian, *Soldering Surf. Mount Technol.* 13, 7 (2001).
10. W.K. Choi and H.M. Lee, *J. Electron. Mater.* 28, 1251 (1999).
11. J.G. Lee, F. Guo, K.N. Subramanian, and J.P. Lucas, *Soldering Surf. Mount Technol.* 14, 11 (2002).
12. M. Li, F. Zhang, W.T. Chen, K. Zeng, K.N. Tu, H. Balkan, and P. Elenius, *J. Mater. Res.* 17, 1612 (2002).
13. D.R. Frear and S. Thomas, *MRS Bull.* 28, 68 (2003).
14. A. Zribi, A. Clark, L. Zavalij, P. Borgesen, and E.J. Cotts, *J. Electron. Mater.* 30, 1157 (2001).
15. C.W. Hwang, J.G. Lee, K. Suganuma, and H. Mori, *J. Electron. Mater.* 32, 52 (2003).
16. K.S. Kim, S.H. Huh, and K. Suganuma, *Microelectron. Reliab.* 43, 259 (2003).
17. W.K. Choi, J.H. Kim, S.W. Jeong, and H.M. Lee, *J. Mater. Res.* 17, 43 (2002).
18. I.E. Anderson, B.A. Cook, J. Harringa, and R.L. Terpstra, *J. Electron. Mater.* 31, 1166 (2002).
19. J.P. Lucas, F. Guo, J. McDougall, T.R. Bieler, K.N. Subramanian, and J.K. Park, *J. Electron. Mater.* 28, 1268 (1999).
20. S.K. Kang and T.G. Ference, *J. Mater. Res.* 8, 1063 (1993).
21. F. Guo, J. Lee, J.P. Lucas, K.N. Subramanian, and T.R. Bieler, *J. Electron. Mater.* 30, 1222 (2001).
22. C.M. Chuang and K.L. Lin, *J. Electron. Mater.* 32, 1426 (2003).
23. J.Y. Tsai, Y.C. Hu, C.M. Tsai, and C.R. Kao, *J. Electron. Mater.* 32, 1203 (2003).
24. M.L. Huang, C.M.L. Wu, and J.K.L. Lai, *J. Mater. Sci. Mater. Elec.* 11, 57 (2000).
25. C.M.L. Wu, M.L. Huang, J.K.L. Lai, and Y.C. Chan, *J. Electron. Mater.* 29, 1015 (2000).
26. M.L. Huang, C.M.L. Wu, J.K.L. Lai, and Y.C. Chan, *J. Electron. Mater.* 29, 1021 (2000).
27. C. Suryanarayana, *Prog. Mater. Sci.* 46, 1 (2001).
28. H.L. Lai and J.G. Duh, *J. Electron. Mater.* 32, 215 (2003).
29. J.S. Benjamin, *Sci. Am.* 234, 40 (1976).
30. S.T. Kao and J.G. Duh, *J. Electron. Mater.* 33, 1445 (2004).
31. R.R. Chromik, R.P. Vinci, S.L. Allen, and M.R. Notis, *J. Mater. Res.* 18, 2251 (2003).
32. G.Y. Jang, J.W. Lee, and J.G. Duh, *J. Electron. Mater.* 33, 1103 (2004).
33. L. Lu, M.O. Lai, and S. Zhang, *J. Mater. Process. Technol.* 67, 100 (1997).